Entropy generation on MHD Eyring-Powell hybrid nanofluid flow over a curved stretching sheet with shape factors and the Cattaneo–Christov heat flux model: A comparative study

K. Sakkaravarthi, P. Bala Anki Reddy*
Department of Mathematics, S.A.S., Vellore Institute of Technology (VIT), Vellore-632014, India.
* Corresponding author E-mail: pbarmaths@gmail.com

Abstract

This article focuses on the influence of the shape factor of entropy generation on the MHD flow of an Eyring–Powell hybrid nanofluid past a permeable over a curved stretched sheet with Cattaneo–Christov heat flux. Using the Homotopy Perturbation Method (HPM) and the shooting method, the governing nonlinear coupled PDEs are converted into ODEs with similarity variables and solved (R-K 4th order). Magnetic field, mixed convection, Eyring-Powell fluid, thermal relaxation, curvature, and thermal radiation are studied and represented in terms of velocity, temperature, entropy production, Bejan number, heat transfer, and coefficients of skin friction. To compare outcomes, we employ the Homotopy Perturbation Method. The Homotopy Perturbation Method produces more precise and reliable results than the numerical method. When a magnetic field affected the hybrid nanofluid as it increased over a curved stretching sheet, the velocity profile decreased. In actuality, the Lorentz force increases as the magnetic field result increases. In the presence of a curved stretching sheet, the velocity profile also decreases as a result of increased magnetic parameters. In the three shapes, the temperature profile rises with increasing thermal radiation values. This model is utilized in biological applications such as MRI, RFA, and cancer therapy.

KEYWORDS MHD; Eyring-Powell fluid; Cattaneo-Christov heat flux; non-linear thermal radiation; Entropy generation.

1. Introduction

The use of nanoparticles (metallic, oxide, non-metallic, and ceramic) has garnered much attention in modern times due to its great applicability in various fields, material science, the food industry, and agriculture. Choi [1] produced nanofluids by adding 1-100 nm-sized particles to regular fluids (blood, ethylene glycol, mineral oil, Biofluids, etc.). It

Present address:
K. Sakkaravarthi, Department of Mathematics, St. Peter's Engineering College, Medchal, Dhulapally Hyderabad - 500100, Telangana, India.

was first proposed. Many researchers have discussed applications of nanofluids in many areas, including engineering, medical apparatus, paper production, mechanical, architecture, drug delivery, scientific processes biomedical, etc. Additionally, a brand-new kind of nanofluids called mixed nanofluids transmit heat more effectively than conventional heat transfer fluid and nanofluid with a single nanoparticle. When more nanoparticles are mixed in with a base fluid, this makes a hybrid nanofluid. Hybrid nanofluids receive significant attention given their extensive applications in electronic cooling, machining, electronic cooling, lubrication, solar heating, warming procedures in buildings, nuclear cooling systems, generator cooling, welding, biomedicine, and targeted drug delivery [2,3]. The silver carriers are then modified in two steps to achieve dual functionalities. Silver nanoparticles are crosslinked with iron oxide nanoparticles (Fe_3O_4) to form Ag-Fe_3O_4 nanocomposites (Fe-Ag). Overall, the superparamagnetic component of Fe_3O_4 nanoparticles will allow the nanocomposites to be magnetized in a magnetic field, providing a preferred magnetic moment that can be carefully controlled against circulation shearing for Drug delivery, medical business as anti-microbial and anti-cancer agents, photothermal theory, pictures, and catalysis. Sperling et al. [4] explained the uses of Gold nanoparticles in biology and heating. Lacerda et al. [5] examined the interaction of gold nanoparticles with common human blood proteins. Numerical research was done on heat transfer analysis using nanofluid flow in a porous medium by Reddy et al. [6]. Abbas et al. [7] conducted a study to examine the MHD, thermal radiation, heat generation, and hybrid(Ag-Cu/pure water) nanofluid flow past a porous media curved sheet with a nonlinear stretching sheet. Babu et al. [8] studied the squeezed flow of polyethylene glycol and water-based hybrid nanofluids over a magnetized sensor surface. The EMHD flow of a nanofluid with a hyperbolic tangent across a stretched sheet was investigated by Asogwa et al. [9]. Sajjan et al. [10] studied the influence of linear, nonlinear, and quadratic Rosseland approximations on the 3D flow behaviour of ternary hybrid nanoparticles of different shapes.

The importance of analyzing magnetohydrodynamics (MHD) flow phenomena and their applications in industries, geology, including geology, attractive medication focuses, astrophysics, geophysics, the drug industry, engineering, magnetic drug targeting, pharmaceuticals, and mechanical engineering—moreover, biomedical, magnetic endoscopy, and cancer tumour treatment. The influence of thermal radiation and heat transfer on CNTs on MHD flow is currently being examined by Mahabaleshwar et al. [11]. Islam et al. [12]

Present address:
K. Sakkaravarthi, Department of Mathematics, St. Peter's Engineering College, Medchal, Dhulapally Hyderabad - 500100, Telangana, India.

discussed optimizing entropy in MHD nanofluid flow over a curved stretching surface. The entropy generation of MHD and radiation, hybrid (*CuO-MgO*/water (50%) + *EG* (50%) nanofluid flow over a curved stretched sheet was studied by Sakkaravarthi and Reddy [13]. Jalili et al. [14] investigated the effect of magnetic and boundary parameters on the flow characteristics analysis of a shrinking sheet of micropolar ferrofluid. The MHD flow of second-grade nano liquid across a convectively heated curved stretched surface was investigated by Reddy et al. [15]. Rauf et al. [16] investigated the effects of nonlinear surface extending on heat transfer and MHD micropolar ferrofluid flow. The magnetohydrodynamic convective streams of tangent hyperbolic nanofluid crossing an elastic texture that is nonlinearly elongating were studied by Sakthi et al. [17].

The process of heat transmission, also known as thermal radiation, involves the transfer of heat energy between two surfaces. In modern-day cycles, MHD production plays an integral part in manufacturing electronic chips and paper plates. The effect of heat radiation in magnetohydrodynamic flow is enormous and becoming more relevant. Research on viscous flow with thermal radiation has a lot of uses in human activities, especially when it comes to heating and cooling, as well as biomedical and clinical therapy. It is also essential in the context of space technology and high-temperature operations. The effects of ferromagnetic fluid flow across a porous stretched sheet were investigated by Jakeer and Reddy [18]. The impact of the chemical reaction and nonlinear thermal radiation hybrid nanofluids on a curved expanding surface has been studied by Ahmed et al. [19]. Sakkaravarthi and Reddy[20] investigated the MHD flow behavior of two- a dimensional Casson hybrid nanofluid over a porous curved stretching sheet. Jalili et al. [21] investigated thermal analysis and pressure drop in non-continuous helical baffles with different helix angles and hybrid nanoparticles.

Many scientists, engineers, and research scholars have worked on the entropy of thermodynamic systems in recent years. Entropy generation, also known as irreversibility, is a critical measure to calculate the effectiveness of an energy system. The analysis of these irreversible effects (heat transfer and flow) uses the standard measurement of entropy creation and depreciation. Entropy generation occurs through transferring heat, thermal radiation, Joule heating, porosity, and viscous dissipation. Utilizes legal entropy minimization and creation measurement methods. In 1979, Bejan [22] investigated the concepts of entropy

Present address:
K. Sakkaravarthi, Department of Mathematics, St. Peter's Engineering College, Medchal, Dhulapally Hyderabad - 500100, Telangana, India.

generation in convective heat transfer and fluid friction issues. He validated that reducing entropy generation may strengthen a thermal system's mechanical design. Due to its wide variety of heat transfer applications, including maximum heat pump system efficiency, thermal exchangers, maximum heat transfer rate, geothermal applications, biological sectors, and filter design, entropy generation is essential. The irreversibility of the Darcy-Forchheimer presence of CNTs by Joule heating effects was investigated using a curved stretching sheet by Hayat et al. [23].

The main intention of this study is no one has been done on the effect of the entropy generation on MHD Eyring-Powell hybrid nanofluid over a porous curved stretching surface in the presence of the non-linear radiation, heat generation, different shape factors, and Cattaneo-Christov heat flux model. So that's why all effects are considered in this model. In this study, blood was used as the base fluid, and *Ag* and Fe_3O_4 were the nanoparticles. Non-linear PDEs are self-similarly transformed into ODEs by using a set of transformations. To solve the homotopy perturbation method is applied. This model has an extensive variety of biomedical applications, including hyperthermia therapeutics and cancer treatment therapeutics. They are advantageous for incorporating magnetic resonance imaging (*MRI*), especially radiofrequency ablation (*RFA*). A magnetic force field is used to diagnose or treat diseases.

2. Mathematical Formulation

Consider the steady, incompressible, two-dimensional, MHD flow of Eyring-Powell hybrid nanofluid with blood as the base fluid *Ag* and Fe_3O_4 are nanoparticles over a porous flow on a curved stretched sheet. We have computed the boundary layer of a hybrid nanofluid traveling over a curved extended surface with a radius *R*. Putting two equal and opposing pressures in the s direction while maintaining the origin and the velocity the $u_w = as(a > 0)$, where a represents the stretch constantly. A magnetic field of strength (B_0) is applied in the perpendicular direction to the flow. As seen in Figure 1, the radius of curvature normalizes the surface's shape. The influences of MHD, nonlinear thermal radiation, and porous media, Joule heating, are all being investigated. Furthermore, the Cattaneo–Christov theory, which is based on thermal relaxation, is also explored for heat transfer. The following are the governing equations: Hayat et al. [24]

Present address:
K. Sakkaravarthi, Department of Mathematics, St. Peter's Engineering College, Medchal, Dhulapally Hyderabad - 500100, Telangana, India.

$$\frac{\partial}{\partial r}(r+R)v+R\frac{\partial}{\partial s}u=0$$

(1)

$$\frac{u^2}{r+R}=\frac{1}{\rho_{hnf}}\frac{\partial}{\partial r}\hat{p}$$

(2)

$$v\frac{\partial u}{\partial r}+\left(\frac{R}{r+R}\right)u\frac{\partial u}{\partial s}+\frac{uv}{r+R}=-\frac{1}{\rho_{hnf}}\left(\frac{R}{r+R}\right)\frac{\partial\hat{p}}{\partial s}+\left(\gamma_{hnf}+\frac{1}{\rho_{hnf}\beta c}\right)\left(\frac{\partial^2 u}{\partial r^2}+\left(\frac{1}{r+R}\right)\frac{\partial u}{\partial r}-\frac{u}{(r+R)^2}\right)$$
$$-\frac{1}{6\rho_{hnf}\beta c^3}\left(\begin{array}{l}3\frac{\partial^2 u}{\partial r^2}\left(\frac{\partial u}{\partial r}\right)^2-\left(\frac{1}{r+R}\right)\left(\frac{\partial u}{\partial r}\right)^3+\frac{3u}{(r+R)^2}\left(\frac{\partial u}{\partial r}\right)^2\\+\frac{3u^2}{(r+R)^2}\frac{\partial^2 u}{\partial r^2}+\frac{u^3}{(r+R)^4}-\frac{6u}{r+R}\frac{\partial u}{\partial r}\frac{\partial^2 u}{\partial r^2}-\frac{3u^2}{(r+R)^3}\frac{\partial u}{\partial r}\end{array}\right)-\frac{\sigma_{hnf}}{\rho_{hnf}}B_0{}^2u+\frac{(\rho\beta)_{hnf}\,g(T-T_\infty)}{\rho_{hnf}}-\frac{\mu_{hnf}}{\rho_{hnf}}\frac{u}{k_p}$$

(3)

$$v\frac{\partial T}{\partial r}+u\left(\frac{R}{r+R}\right)\frac{\partial T}{\partial s}+\lambda_E\psi_E=\left(\begin{array}{l}\frac{k_{hnf}}{(\rho c_p)_{hnf}}\left(\left(\frac{1}{r+R}\right)\frac{\partial T}{\partial r}+\frac{\partial^2 T}{\partial r^2}\right)-\frac{1}{(\rho c_p)_{hnf}}\left(\frac{1}{r+R}\right)\frac{\partial}{\partial r}((r+R)q_r)\\+\frac{\mu_{hnf}}{(\rho c_p)_{hnf}}\left(\frac{\partial u}{\partial r}+\frac{u}{r+R}\right)^2+\frac{\sigma_{hnf}}{(\rho c_p)_{hnf}}B_0{}^2u^2+\frac{1}{(\rho c_p)_{hnf}}Q(T-T_\infty)\exp\left(-\sqrt{\frac{a}{\nu}}\,r\right)\end{array}\right)$$

(4)

Here,

$$\psi_E=\left(\frac{R}{r+R}u\right)\frac{\partial v}{\partial s}\frac{\partial T}{\partial r}+\left(\frac{R^2}{(r+R)^2}u\right)\frac{\partial u}{\partial s}\frac{\partial T}{\partial s}+v\frac{\partial v}{\partial r}\frac{\partial T}{\partial r}+2\frac{uv}{r+R}\frac{\partial^2 T}{\partial r\partial s}+\frac{vR}{r+R}\frac{\partial u}{\partial r}\frac{\partial T}{\partial s}-\frac{uv}{(r+R)^2}\frac{\partial T}{\partial s}+\frac{u^2}{(r+R)^2}\frac{\partial^2 T}{\partial s^2}+v^2\frac{\partial^2 T}{\partial r^2}$$

boundary conditions

Present address:
K. Sakkaravarthi, Department of Mathematics, St. Peter's Engineering College, Medchal, Dhulapally Hyderabad - 500100, Telangana, India.

$$\left.\begin{aligned} & v = v_w, \quad u = as + L\left(\frac{\partial}{\partial r}u - \frac{1}{r+R}u\right), -k\left(\frac{\partial T}{\partial r}\right) = h_f\,(T_w - T) \qquad as\ \ r \to 0 \\ & \frac{\partial u}{\partial r} \to 0, \qquad u \to 0, \quad T = T_\infty \qquad\qquad as\ \ r \to \infty. \end{aligned}\right\}$$

(5)

Thermophysical models follow as ref.[25]

$$\rho_{hnf} = (1-\phi_2)\left((1-\phi_1)\rho_{bf} + \phi_1\rho_{1s}\right) + \phi_2\rho_{2s}$$
$$(\rho c_p)_{hnf} = (1-\phi_2)\left((\rho c_p)_{bf}\,(1-\phi_1) + \phi_1(\rho c_p)_{1s}\right) + (\rho c_p)_{2s}\phi_2$$
$$(\rho\beta)_{hnf} = (1-\phi_2)(1-\phi_1)(\rho\beta)_{bf} + \phi_1(\rho\beta)_{1s} + \phi_2(\rho\beta)_{2s}$$

$$\mu_{hnf} = \frac{\mu_f}{(1-\phi_1)^{2.5}(1-\phi_2)^{2.5}}, \alpha_{hnf} = \frac{k_{hnf}}{(\rho c_p)_{hnf}}, \upsilon_{hnf} = \frac{\mu_{hnf}}{\rho_{hnf}}.$$

$$\frac{\sigma_{hnf}}{\sigma_f} = 1 + \frac{3\left(\frac{(\phi_2\sigma_{2s} + \phi_1\sigma_{1s})}{\sigma_{bf}} - (\phi_2 + \phi_1)\right)}{\left(\frac{(\sigma_{2s}\phi_2 + \sigma_{1s}\phi_1)}{\phi\sigma_{bf}} + 2\right) - \left(\frac{(\sigma_{2s}\phi_2 + \sigma_{1s}\phi_1)}{\sigma_{bf}} + (\phi_2 + \phi_1)\right)}$$

$$\frac{k_{hnf}}{k_{bf}} = \frac{k_{2s} + (m-1)k_{bf} - (m-1)\phi_2 + (k_{bf} - k_{2s})}{k_{2s} + (m-1)k_{bf} + \phi_2(k_{bf} - k_{2s})},$$
$$\frac{k_{bf}}{k_f} = \frac{k_{1s} + (m-1)k_f - (m-1)\phi_1 + (k_f - k_{1s})}{k_{1s} + (m-1)k_f + \phi_1(k_f - k_{1s})},$$

(6)

The following similarity transmutations are taken into consideration:

$$v = -\left(\frac{R}{r+R}\right)\sqrt{a\upsilon_f}\,f(\eta), \qquad u = saf'(\eta), \qquad T = T_\infty\left[1 + (\theta_w - 1)\theta(\eta)\right],$$

$$\hat{p} = \rho_f a^2 s^2 P(\eta),\ \eta = \sqrt{\frac{a}{\upsilon_f}}r.$$

(7)

Equations (2) - (5) are simplified using Equation (7) as follows:

Present address:
K. Sakkaravarthi, Department of Mathematics, St. Peter's Engineering College, Medchal, Dhulapally Hyderabad - 500100, Telangana, India.

$$P' = A_3 \frac{f'^2}{(\eta + K)}$$

(8)

$$\frac{2K}{\eta+K}\frac{P}{A_3} = \frac{1}{A_2}(1+\chi_1)\left(f''' - \frac{f'}{(\eta+K)^2} + \frac{f''}{\eta+K} \right) - \chi_1\chi_2 \left(\begin{array}{l} 3f''^2 f''' + \frac{3f'^2 f'''}{(\eta+K)^2} + \frac{3f''^2 f'}{(\eta+K)^2} - \frac{3f'^2 f''}{(\eta+K)^3} \\ -\frac{6f' f'' f'''}{(\eta+K)} - \frac{f''^3}{\eta+K} + \frac{f'^3}{(\eta+K)^4} \end{array} \right) \qquad (9)$$

$$-\frac{f' f'''}{\eta+K} - \frac{K(f'^2)}{(\eta+K)} + \frac{K(ff'')}{(\eta+K)} + \frac{K(ff')}{(\eta+K)^2} - \frac{A_4}{A_3} M\ f' + \frac{A_5}{A_3}\lambda\theta - \frac{S_k}{A_2} f'$$

Here Radiative heat flux is q_r. The Taylor series linear function T^4 continues to be a temperature. Higher orders are not considered T. $T^4 \cong 4T_\infty^{\ 3}T - 3T_\infty^{\ 4}$. If $S > 0$ is the suction and $S < 0$ is the injection, M is the Magnetic field parameter, λ is the mixed convection parameter, K is the curvature parameter, Pr is the Prandtl number, λ_1 is the heat generation/absorption parameter, Ec is the Eckert number, Rd is the thermal Radiation parameter, S_k is the porosity parameter, γ is the Thermal relaxation parameter and χ_1, χ_2 Eyring-Powell parameters are is given mathematically as follows:

$$\left.\begin{array}{l} q_r = \frac{-4\sigma^*}{3k^*}\frac{\partial T^4}{\partial r},\ M = \frac{\sigma_f B_0^{\ 2}}{a\rho_f},\ \lambda = \frac{g(T_w - T_\infty)}{a^2 s},\ K = \sqrt{\frac{a}{\upsilon_f}}R, Ec = \frac{a^2 s^2}{c_p(T_w - T_\infty)}, \Pr = \frac{\upsilon_f}{\alpha}, \\ \alpha = \frac{k_f}{(\rho c_p)_f}, \lambda_1 = \frac{Q}{a(\rho c_p)_f}, Rd = \frac{16\sigma^* T_\infty^{\ 3}}{k_f 3k^*}, EcPr = Br, S_k = \frac{\nu_f}{k_p}, \gamma = \lambda_E a, \theta_w = \frac{T_w}{T_\infty} \\ \chi_1 = \frac{1}{(\mu\beta c)}, \chi_2 = \frac{a^3 s^2}{6(\nu_f c^2)}, \end{array}\right\}$$

(10)

Equations (8) and (9) can be resolved without taking the pressure into account

$$(1+\chi_1)\left(f^{iv} + 2\frac{f'''}{\eta+K} - \frac{f''}{(\eta+K)^2} + \frac{f'}{(\eta+K)^3} \right) + A_2 \left(\begin{array}{l} \frac{K}{\eta+K}(f'''f - f''f') + \left(\frac{K}{(\eta+K)^2}\right)(f''f - (f'^2)) \\ -\frac{K}{(\eta+K)^3} f'f \end{array} \right)$$

$$+3A_2\chi_1\chi_2\left(\frac{2f'f''f^{iv}}{K+\eta} - \frac{f''^2 f^{iv}}{(K+\eta)^2} - f''^2 f^{iv} \right) + \frac{A_2\chi_1\chi_2}{(K+\eta)}\left(6f'''f''^2 + 6(f''')^2 f' \right) - \frac{A_2\chi_1\chi_2}{(K+\eta)^2}\left(12f''f'f''' + 3(f''')^3 \right)$$

$$-\frac{9A_2\chi_1\chi_2}{(K+\eta)^4} f'^2 + \frac{3A_2\chi_1\chi_2}{(K+\eta)^5} f'^3 + \frac{9A_2\chi_1\chi_2}{(K+\eta)^3}\left(6f'''f'^2 + 9f'f''^2 \right) - 6A_2\chi_1\chi_2(f''')^2 f'' - A_1A_4M\left(\frac{f'}{(\eta+K)} + f'' \right)$$

$$-S_k\left(\frac{f'}{(\eta+K)} + f'' \right) + A_1A_5\lambda\left(\theta' + \frac{1}{(\eta+K)}\theta \right) = 0$$

(11)

Present address:
K. Sakkaravarthi, Department of Mathematics, St. Peter's Engineering College, Medchal, Dhulapally Hyderabad - 500100, Telangana, India.

$$\left(\theta''+\frac{\theta'}{\eta+K}\right)\left(1+\frac{Rd}{A_7}\left(1+\left(\theta_w-1\right)\theta\right)^3\right)+\frac{3Rd}{A_7}\left[\left(1+\left(\theta_w-1\right)\theta\right)^2\right]\theta'^2+\frac{A_6}{A_7}Pr\left(\frac{K}{\eta+K}\right)f\theta'$$
$$+\frac{Br}{A_1A_7}\left(f''+\frac{f'}{\eta+K}\right)^2-\frac{\Pr}{A_7}\gamma\left(\frac{K^2}{\left(\eta+K\right)^2}\left(f^2\theta''+ff'\theta'\right)-K^2f^2\theta'\right)+\frac{A_4}{A_7}BrM\left(f'\right)^2+\frac{Pr}{A_7}\lambda_1\exp(-\eta)\theta=0 \quad (12)$$

In the above equations, we regard

$$A_1=\frac{\mu_{hnf}}{\mu_f},A_2=\frac{\mu_{hnf}}{\mu_f}.\frac{\rho_{hnf}}{\rho_f},A_3=\frac{\rho_{hnf}}{\rho_f},A_4=\frac{\sigma_{hnf}}{\sigma_f},A_5=\frac{(\rho\beta)_{hnf}}{(\rho\beta)_f},A_6=\frac{\left(\rho c_p\right)_{hnf}}{\left(\rho c_p\right)_f},A_7=\frac{k_{hnf}}{k_f}$$

boundary conditions

$$\left.\begin{aligned}&f(0)=S,\ -\theta'(0)=Bi(1-\theta(0)),\quad f'(0)=1+L_s\left(f''(0)-\frac{f'(0)}{K}\right)\\&f''(\infty)=0,\quad f'(\infty)=0,\quad \theta(\infty)=0.\end{aligned}\right\} \quad (13)$$

3. Development of Entropy Generation

The second law of thermodynamics defines entropy formation as the irreversible process of hybrid nanofluid flow over the curved stretching sheet. Many organizations, including viscous forces, thermal radiation, porosity, and low-driven force, create normal entropy generation. The creation of entropy may be used to calculate the amount of energy wasted during a task. There are several liquid models. Entropy-reducing systems. The model optimizes entropy in the current flow issue:

3.1. *Entropy generation*

The entropy development in a dimensional form is

$$E_G=\frac{k_{hnf}}{T_\infty^{\ 2}}\left(1+\frac{16\sigma^*T^3}{k_f3k^*}\right)\left(\frac{\partial T}{\partial r}\right)^2+\frac{\mu_{hnf}}{T_\infty}\left(\frac{\partial u}{\partial r}+\frac{u}{r+R}\right)^2+\frac{\mu_{hnf}}{T_\infty k_p}u^2+\frac{\sigma_{hnf}}{T_\infty}B_0^{\ 2}u^2$$

(14)

Dimensionless form is

Present address:
K. Sakkaravarthi, Department of Mathematics, St. Peter's Engineering College, Medchal, Dhulapally Hyderabad - 500100, Telangana, India.

$$S_G = A_7\alpha_1\theta'^2\left(1+Rd\left(1+\left(\theta_w-1\right)\theta\right)^3\right)+\frac{Br}{A_1}\left(f''+\frac{f'}{\eta+K}\right)^2+A_4BrM\left(f'\right)^2+\frac{S_kBrf^{1^2}}{A_1}$$

(15)

3.2. *Bejan number*

The Bejan number, which also has to be written as

$$Be=\frac{A_7\alpha_1\theta'^2\left(1+Rd\left(1+\left(\theta_w-1\right)\theta\right)^3\right)}{A_7\alpha_1\theta'^2\left(1+Rd\left(1+\left(\theta_w-1\right)\theta\right)^3\right)+\frac{Br}{A_1}\left(f''+\frac{f'}{\eta+K}\right)^2+A_4BrM\left(f'\right)^2+\frac{S_kBrf^{1^2}}{A_1}}$$

(16)

Designates the Brinkman number $Br=\frac{\mu_{hnf}(as)^2}{k_f\left(T_w-T_\infty\right)}$, Total entropy rate $S_G=\frac{E_GT_\infty\upsilon_f}{ak_f\left(T_w-T_\infty\right)}$,

Temperature ratio parameter $\alpha_1=\frac{\Delta T}{T_\infty}=\frac{T_w-T_\infty}{T_\infty}$.

4. Physical Quantities

4.1. *A measure of skin friction coefficient*

One of the physical factors of importance is the skin friction coefficient along the s-directions $C_{fs}=\frac{\tau_{rs}}{\rho(u_w)^2}$. As follows is a representation of shear stress:

$$\tau_{rs}=\left(\left(\mu+\frac{1}{\beta c}\right)\left(\frac{\partial u}{\partial r}-\frac{u}{r+R}\right)-\frac{1}{6\beta c^3}\left(\left(\frac{\partial u}{\partial r}\right)^3-\frac{u^3}{\left(r+R\right)^3}+\frac{3u^2}{\left(r+R\right)^2}\left(\frac{\partial u}{\partial r}\right)-\frac{3u}{r+R}\left(\frac{\partial u}{\partial r}\right)^2\right)\right)_{r=0}$$

(17)

then we have

$$C_{fs}\,\mathrm{Re}_s^{1/2}=\left(1+\chi_1\right)\left[f''(0)-\frac{f'(0)}{K}\right]-\chi_1\chi_2\left(f'''(0)-\frac{3f''^2(0)f'(0)}{K}+\frac{3f''(0)f'^2(0)}{K^2}-\frac{f'^3}{K^3}\right) \quad (18)$$

4.2. *Nusselt number*

Present address:
K. Sakkaravarthi, Department of Mathematics, St. Peter's Engineering College, Medchal, Dhulapally Hyderabad - 500100, Telangana, India.

The physical quantities of interest are a rate of heat transfer along the *s*-directions, which are given as $Nu_s = \frac{sq_w}{k_f\left(T_w - T_\infty\right)}$ (19)

Where q_w is *the* heat flux at the surface in the *s*-direction, which is given by

$q_w = \left(\left(q_r\right)_w - \frac{\partial T}{\partial r} \right)_{r=0}$ then we have

$$Nu_s \, \mathrm{Re}_s^{-1/2} = -\left(\frac{k_{hnf}}{k_f} + Rd\left(1 + \left(\theta_w - 1\right)\theta\left(0\right)\right)^3 \right)\theta'(0) \quad (20)$$

Where $\mathrm{Re}_s^{1/2} = \sqrt{\frac{a}{\upsilon_f}}s$ the local Reynolds number.

5. Methodology

This section will present the Homotopy approach before going through the suggested issue. This approach was first out by Mr. He [26] in 1998, and it has been utilized to solve nonlinear ODEs. The technique of generic boundary element was created in 2004 when he combined this approach with the boundary element method. The process is as follows: A series of guesses may be obtained via Homotopy Perturbation, and a further series of replies can be obtained that are incrementally closer and closer to the correct answer. This approach takes advantage of, among other things, traits like action flexibility when choosing the linear operator and initial function. A big nonlinear issue may be solved and split into smaller, simpler linear problems with the same level of action and beginning option flexibility. The controllability of the convergence region is another advantage of this methodology, making it stand out from other approaches addressed by Shqair [27].

5.1. ***HPM*** *approach*

Consider the following non-linear ODEs of the system to determine the HPM concept:

$$\mathrm{E}\left(\omega\right) - \mathrm{T}\left(z\right) = 0, \quad z \in \varphi$$

(21)

Present address:
K. Sakkaravarthi, Department of Mathematics, St. Peter's Engineering College, Medchal, Dhulapally Hyderabad - 500100, Telangana, India.

boundary conditions are

$$\psi\left(\omega, \frac{\partial\omega}{\partial n}\right)=0,\ \ z\in\partial\varphi$$

(22)

The formation of the HPM is given as follows:

$$H\left(\ \omega, p\right)=\left(1-p\right)\left(L\left(\omega\right)-L\left(\omega_0\right)\right)+p\ \left[\mathrm{E}\left(\omega\right)-T\left(z\right)\right]=0$$

(23)

Were,

$$\omega\left(z, p\right):\varphi\times\left[0,1\right]\rightarrow R_1$$

(24)

At which $p\in\left[0,1\right]$ is a parameter for fixed and in this function (ω_0), the boundary conditions are recorded, it is now Eq. (21) most important.

To express the previous solution, in the power series in *p*:

$$\omega=\omega_0+p\omega_1+p^2\omega_2+p^3\omega_3+...$$

(25)

As an exact approximation, the solution is $p=1$.

$$\omega=\omega_0+\omega_1+\omega_2+\omega_3+...$$

(26)

5.2. ***HPM is implemented in this method:***

Equations (11) and (12) of the (HPM) model can be expressed as follows using the equations above

Present address:
K. Sakkaravarthi, Department of Mathematics, St. Peter's Engineering College, Medchal, Dhulapally Hyderabad - 500100, Telangana, India.

$$(1-p)f^{iv}+p\left(\begin{array}{l}(1+\chi_1)\left(f^{iv}+2\frac{f'''}{\eta+K}-\frac{f''}{(\eta+K)^2}+\frac{f'}{(\eta+K)^3}\right)+A_2\left(\begin{array}{l}\frac{K}{\eta+K}\left(f'''f-f''f'\right)+\left(\frac{K}{(\eta+K)^2}\right)\left(f''f-f'^2\right)\\-\frac{K}{(\eta+K)^3}f'f\end{array}\right)\\+3A_2\chi_1\chi_2\left(\frac{2f'f''f^{iv}}{K+\eta}-\frac{f''^2f^{iv}}{(K+\eta)^2}-f''^2f^{iv}\right)+\frac{A_2\chi_1\chi_2}{(K+\eta)}\left(6f'''f''^2+6f'''^2f'\right)-\frac{A_2\chi_1\chi_2}{(K+\eta)^2}\left(12f''f'f'''+3f'''^3\right)\\-\frac{9A_2\chi_1\chi_2}{(K+\eta)^4}f'^2+\frac{3A_2\chi_1\chi_2}{(K+\eta)^5}f'^3+\frac{9A_2\chi_1\chi_2}{(K+\eta)^3}\left(6f'''f'^2+9f'f''^2\right)-6A_2\chi_1\chi_2f'''^2f''-A_1A_4M\left(\frac{f'}{(\eta+K)}+f''\right)\\-S_k\left(\frac{f'}{(\eta+K)}+f''\right)+A_1A_5\lambda\left(\theta'+\frac{1}{(\eta+K)}\theta\right)\end{array}\right)=0$$

(27)

$$(1-p)\left(1+\frac{1}{A_7}Rd\right)\theta''+p\left(\begin{array}{l}\left(\theta''+\frac{\theta'}{\eta+K}\right)\left(1+\frac{Rd}{A_7}\left(1+(\theta_w-1)\theta\right)^3\right)+\frac{3Rd}{A_7}\left[\left(1+(\theta_w-1)\theta\right)^2\right]\theta'^2\\+\frac{A_6}{A_7}Pr\left(\frac{K}{\eta+K}\right)f\theta'-\frac{\Pr}{A_7}\gamma\left(\frac{K^2}{(\eta+K)^2}\left(f^2\theta''+ff'\theta'\right)-K^2f^2\theta'\right)\\+\frac{Br}{A_1A_7}\left(f''+\frac{f'}{\eta+K}\right)^2+\frac{A_4}{A_7}BrM\left(f'\right)^2+\frac{Pr}{A_7}\lambda_1\exp(-\eta)\theta\end{array}\right)=0$$

(28)

boundary conditions

$$\left.\begin{array}{l}f(0)=S,\ -\theta'(0)=Bi(1-\theta(0)),\quad f'(0)=1+L_s\left(f''(0)-\frac{f'(0)}{K}\right)\\f''(\infty)=0,\quad f'(\infty)=0,\quad \theta(\infty)=0.\end{array}\right\}$$

(29)

$f(\eta)$ and $\theta(\eta)$ are considered in the standard power series,

$$f(\eta)=f_0(\eta)+pf_1(\eta)+p^2f_2(\eta)+p^3f_3(\eta)+\ldots$$

(30)

$$\theta(\eta)=\theta_0(\eta)+p\theta_1(\eta)+p^2\theta_2(\eta)+p^3\theta_3(\eta)+\ldots$$

Present address:
K. Sakkaravarthi, Department of Mathematics, St. Peter's Engineering College, Medchal, Dhulapally Hyderabad - 500100, Telangana, India.

Equations (30) and (31) should be replaced with Equations (27)-(29), and the linear equation solution is obtained by comparing the coefficients of similar p-term powers, with the following effect:

$$f_0 = f_0'''\chi_1 + f_0''' = 0$$

$$\theta_0 = \frac{\theta_0''\, Rd\ \theta_w^{\,3}}{A_7} - \frac{\theta_0''\,\gamma\ \mathrm{Pr}}{A_7} + 4\theta_0'' = 0$$

(31)

When conditions of zeros-order apply,

$$f_0(0) = S,\ f_0'(0) = 1 + L_s\left(f_0''(0) - \frac{f_0'(0)}{K}\right),\ f_0''(1) = 0,\ f_0'(1) = 0.$$

(32)

$$\theta_0(0) = -Bi(1-\theta_0(0)), \theta_0(1) = 0$$

First-order,

$$f_1 = \frac{A_1A_5\lambda\theta_0'}{(\eta+K)} - \frac{A_2A_5Kf_0'^2}{(\eta+K)^2} - A_1A_4Mf_0 + A_1A_5\lambda\theta_0' + \frac{6A_2\chi_1\chi_2 f_0'f_0''f_0^{iv}}{(\eta+K)^2} - \frac{12A_2\chi_1\chi_2 f_0'f_0''f_0'''}{(\eta+K)^2}$$
$$- \frac{3A_2\chi_1\chi_2 f_0'^2 f_0^{iv}}{(\eta+K)} + \frac{6A_2\chi_1\chi_2 f_0''^2 f_0'''}{(\eta+K)} + \frac{6A_2\chi_1\chi_2 f_0'''^2 f_0'}{(\eta+K)} - \frac{9A_2\chi_1\chi_2 f_0'^2 f_0''}{(\eta+K)^4} + \frac{6A_2\chi_1\chi_2 f_0'''f_0'^2}{(\eta+K)^2}$$
$$+ \frac{9A_2\chi_1\chi_2 f_0''^2 f_0'}{(\eta+K)^3} + f_1^{iv} + f_1^{iv}\chi_1 + \frac{2\chi_1 f_0'''}{(\eta+K)} - \frac{\chi_1 f_0''}{(\eta+K)^2} + \frac{\chi_1 f_0'}{(\eta+K)^3} - \frac{S_k f_0'}{(\eta+K)} - \frac{f_0''}{(\eta+K)^2}$$
$$+ \frac{f_0'}{(\eta+K)^3} - S_k f_0'' + \frac{2f_0'''}{(\eta+K)} + \frac{A_2Kf_0f_o'''}{(\eta+K)} - \frac{A_2Kf'_0f_o''}{(\eta+K)} + \frac{A_2Kf_0f_o''}{(\eta+K)^2} - \frac{A_2Kf_0f_o'}{(\eta+K)^3} - -\frac{A_1A_4Mf_o'}{(\eta+K)}$$
$$-3A_2\chi_1\chi_2 f_0^{iv}f_0''^2 - 6A_2\chi_1\chi_2 f_0'''^2 f_0'' - \frac{3A_2\chi_1\chi_2 f_0'''^3}{(\eta+K)^2} + \frac{3A_2\chi_1\chi_2 f_0'^3}{(\eta+K)^5} = 0$$

Present address:
K. Sakkaravarthi, Department of Mathematics, St. Peter's Engineering College, Medchal, Dhulapally Hyderabad - 500100, Telangana, India.

(33)

$$\theta_1 = -\frac{Rd\theta_W{}^3\theta_0''}{A_7} + \frac{Pr\,\gamma\,\theta_0''}{A_7} + \frac{Rd\theta_W{}^3\theta_1''}{A_7} - \frac{\Pr\gamma\theta_1''}{A_7} + \frac{Rd\;\theta_0'}{A_7(\eta+K)} + \frac{Brf_0''^2}{A_7A_1} - 3\frac{Rd\theta_0{}^2\theta_0''}{A_7}$$
$$-3\frac{Rd\;\theta_0\theta_0''}{A_7} - \frac{Rd\;\theta_0{}^3\theta_0''}{A_7} + \frac{3Rd\;\theta_0{}^2\theta_0'^2}{A_7} - \frac{6Rd\;\theta_0\theta_0'^2}{A_7} + \frac{\lambda_1\exp(-\eta)\theta_0}{A_7} + \frac{\Pr A_6 K f_0\theta_0'}{A_7(\eta+K)} + \frac{2Brf_0''f_0'}{A_7A_1\beta(\eta+K)}$$
$$+\frac{Rd\theta_W{}^3\theta_0'\theta_0^3}{A_7(\eta+K)} + \frac{Br\;f_0'^2}{A_7A_1\beta(\eta+K)^2} + \frac{\gamma\Pr K^2\;f_0{}^2\theta_0^1}{A_7} + \frac{3Rd\;T_w\theta_0{}^2\theta_0'}{A_7(\eta+K)} - \frac{6Rd\;T_w\theta_0{}^2\theta_0'}{A_7(\eta+K)} - \frac{3Rd\;T_w\theta_0{}^3\theta_0'}{A_7(\eta+K)}$$

$$+\frac{3Rd\;T_w{}^2\theta_0'}{A_7(\eta+K)} + \frac{3Rd\;T_w\theta_0{}^3\theta_0'}{A_7(\eta+K)} + \frac{2Brf_0''f_0'}{A_7A_1(\eta+K)} + 4\theta_1'' + \frac{3Rd\;\theta_0'^2}{A_7} - 3\theta_0'' + \frac{\theta_0'}{\eta+K} + \frac{3Rd\;T_w\theta_0\theta_0''}{A_7}$$
$$-\frac{6RdT_w\theta_0''\theta_0{}^2}{A_7} - \frac{3RdT_w{}^2\theta_0{}^3\theta_0''}{A_7} + \frac{3RdT_w\theta_0{}^3\theta_0''}{A_7} + \frac{3Rd\theta_0{}'\theta_0{}^2}{A_7(\eta+K)} - \frac{3Rd\theta_0\theta_0'}{A_7(\eta+K)} - \frac{6T_wRd\theta_0{}'\theta_0'^2}{A_7} \qquad (34)$$
$$+\frac{3Rd\;T_w{}^2\theta_0{}^2\theta_0'^2}{A_7(\eta+K)} - \frac{6Rd\;T_w\theta_0{}^2\theta_0'^2}{A_7} + \frac{Rd\;T_w{}^2\theta_0{}^3\theta_0''}{A_7} + \frac{A_4M\;Br\;f_0'^2}{A_7} + \frac{Br\;f_0''^2}{A_7A_1\beta} - \frac{\gamma\Pr K^2 f_0'\theta_0'}{A_7(\eta+K)^2} = 0$$

Boundary conditions are

$$f_0(0) = S,\ f_1'(0) = 1 + L_s\left(f_1''(0) - \frac{f_1'(0)}{K}\right),\ f_1''(1) = 0,\ f_1'(1) = 0.$$

$$\theta_1(0) = -Bi(1-\theta_1(0)), \theta_1(1) = 0 \qquad (35)$$

Second-order

Present address:
K. Sakkaravarthi, Department of Mathematics, St. Peter's Engineering College, Medchal, Dhulapally Hyderabad - 500100, Telangana, India.

$$f_2 = \frac{A_1A_5\lambda\theta_1}{(\eta+K)} + A_1A_5\lambda\theta_1' - A_1A_4Mf_1'' - \frac{f_1''}{(\eta+K)^2} + \frac{2f_1''}{\eta+K} + \frac{\chi_1 f_1'}{(\eta+K)^3} + \frac{2\chi_1 f_1''}{(\eta+K)} - \frac{\chi_1 f_1''}{(\eta+K)^2}$$
$$- S_k f_1'' - \frac{S_k f_1'}{(\eta+K)} + f_2^{iv} + \frac{A_2Kf_1f_0'''}{(\eta+K)} + \frac{A_2Kf_0f_1''}{(\eta+K)^2} - \frac{A_2Kf_0'f_1''}{(\eta+K)} - \frac{A_2Kf_1'f_0''}{(\eta+K)} - \frac{2A_2Kf_0'f_1''}{(\eta+K)^2}$$
$$- \frac{A_2Kf_1f_0'}{(\eta+K)^3} + \frac{-A_1A_4Mf_1'}{(\eta+K)} - 3A_2\chi_1\chi_2 f_1^{iv} f_0''^2 - 6A_2\chi_1\chi_2 f_0''^2 f_1'' + \frac{A_2Kf_0f_1'''}{(\eta+K)} + \frac{f_1'}{(\eta+K)^3}$$
$$- \frac{3A_2\chi_1\chi_2 f_0'^2 f_1^{iv}}{(\eta+K)} - 3A_2\chi_1\chi_2 f_0^{iv} f_0'' f_1'' + \frac{6A_2\chi_1\chi_2 f_0''^2 f_1'''}{(\eta+K)} + \frac{6A_2\chi_1\chi_2 f_0'''^2 f_1''}{(\eta+K)} + \chi_1 f_2^{iv}$$
$$-12A_2\chi_1\chi_2 f_0''' f_1''' f_0'' - \frac{9A_2\chi_1\chi_2 f_0'^2 f_1''}{(\eta+K)^4} + \frac{9A_2\chi_1\chi_2 f_0'^2 f_1'}{(\eta+K)^5} - \frac{12A_2\chi_1\chi_2 f_0' f_1'' f_0'''}{(\eta+K)^2}$$
$$- \frac{9A_2\chi_1\chi_2 f_0'''^2 f_1'''}{(\eta+K)^2} + \frac{9A_2\chi_1\chi_2 f_1' f_0'''^2}{(\eta+K)^3} + \frac{6A_2\chi_1\chi_2 f_1' f_0'' f_0^{iv}}{(\eta+K)^2} - \frac{6A_2\chi_1\chi_2 f_1' f_0' f_0^{iv}}{(\eta+K)}$$
$$+ \frac{12A_2\chi_1\chi_2 f_0'' f_1'' f_0'''}{(\eta+K)} + \frac{12A_2\chi_1\chi_2 f_0''' f_1''' f_0'}{(\eta+K)} - \frac{12A_2\chi_1\chi_2 f_0' f_0'' f_1'''}{(\eta+K)^2} + \frac{6A_2\chi_1\chi_2 f_1''' f_0'^2}{(\eta+K)^3}$$
$$- \frac{12A_2\chi_1\chi_2 f_1' f_0'' f_0'''}{(\eta+K)^2} - \frac{18A_2\chi_1\chi_2 f_0' f_1' f_0''}{(\eta+K)^4} + \frac{12A_2\chi_1\chi_2 f_0''' f_0' f_1'}{(\eta+K)^3} + \frac{18A_2\chi_1\chi_2 f_0' f_0'' f_1''}{(\eta+K)^3} \qquad (36)$$
$$+ \frac{6A_2\chi_1\chi_2 f_0' f_0'' f_1^{iv}}{(\eta+K)^2} + \frac{6A_2\chi_1\chi_2 f_0' f_1'' f_1^{iv}}{(\eta+K)^2} = 0$$

$$\theta_2 = -\frac{Rd\theta_w^3\theta_1''}{A_7} + \frac{Pr\,\gamma\,\theta_1''}{A_7} + \frac{Rd\,\theta_1'}{A_7(\eta+K)} - 3\frac{Rd\,\theta_0^2\theta_1''}{A_7} - 3\frac{Rd\,\theta_0\theta_1''}{A_7} + \frac{Rd\,\theta_0^3\theta_0''}{A_7} - \frac{Rd\theta_w^3\theta_1''}{A_7}$$
$$- \frac{6Rd\,\theta_1\theta_0'^2}{A_7} + \frac{\lambda_1\exp(-\eta)\theta_1}{A_7} + \frac{\Pr A_6K f_0\theta_1'}{A_7(\eta+K)} + \frac{\Pr A_6K f_1\theta_0'}{A_7(\eta+K)} + \frac{6Rd\,T_w^2\theta_0\theta_1\theta_0'}{A_7(\eta+K)} - \frac{12Rd\,T_w\theta_0\theta_1\theta_0'}{A_7(\eta+K)} +$$
$$- \frac{9Rd\,T_w^2\theta_0^2\theta_1\theta_0'}{A_7(\eta+K)} + \frac{9Rd\,T_w\theta_0^2\theta_1\theta_0'}{A_7(\eta+K)} + \frac{2Brf_0''f_1'}{A_7A_1\beta(\eta+K)} + \frac{2Brf_1''f_0'}{A_7A_1\beta(\eta+K)} + \frac{2Brf_0''f_1'}{A_7A_1\beta(\eta+K)^2}$$
$$+ \frac{6Rd\,\theta_0'\theta_1'}{A_7} + \frac{3Rd\,T_w^3\theta_0^2\theta_1\theta_0'}{A_7(\eta+K)} + \frac{\gamma\Pr K^2 f_0^2\theta_1''}{A_7(\eta+K)^2} - \frac{\gamma\Pr K^2 f_0'^2\theta_1'}{A_7(\eta+K)^2} + \frac{\gamma\Pr K^2 f_0 f_1\theta_0'}{A_7} + \frac{RdT_w^3\theta_0^3\theta_1'}{A_7(\eta+K)}$$

$$+ \frac{\gamma\Pr K^2 f_0'^2\theta_1'}{A_7} + \frac{\gamma\Pr K^2 f_0^2\theta_1'}{A_7} + \frac{3RdT_w\,t_1\theta_0'}{A_7(\eta+K)} + \frac{6Rd\theta_0\,\theta_1\theta_0'}{A_7(\eta+K)} - \frac{3Rd\theta_0^2\,\theta_1\theta_0'}{A_7(\eta+K)} + \frac{3RdT_w\theta_0\,\theta_1}{A_7(\eta+K)}$$
$$+ \frac{3RdT_w^2\theta_0^2\,\theta_1'}{A_7(\eta+K)} - \frac{6RdT_w\theta_0^2\,\theta_1'}{A_7(\eta+K)} - \frac{3RdT_w^2\theta_0^3\,\theta_1'}{A_7(\eta+K)} + \frac{3RdT_w^2\theta_0^3\,\theta_1'}{A_7(\eta+K)} + \frac{6RdT_w^2\theta_0\theta_1\,\theta_1'}{A_7} - \frac{12RdT_w\theta_0\theta_1\,\theta_0''}{A_7}$$
$$+ \frac{3RdT_w^3\theta_0^2\theta_1\,\theta_0''}{A_7} - \frac{9RdT_w^2\theta_0^2\theta_1\,\theta_0''}{A_7} + \frac{9RdT_w\theta_0^2\theta_1\,\theta_0''}{A_7} + \frac{2Brf_0''f_1'}{A_7A_1(\eta+K)} + \frac{2Brf_1''f_0'}{A_7A_1(\eta+K)} + \frac{2Brf_0'f_1'}{A_7A_1(\eta+K)^2}$$
$$+ \frac{2Brf_0''f_1'}{A_7A_1(\eta+K)^2} + \frac{2f_0''f_1'}{A_7A_1\beta} + \frac{2A_4MBrf_0'f_1'}{A_7} + \frac{12RdT_w\theta_0\theta_1'\,\theta_0'}{A_7} + \frac{6RdT_w^2\theta_0^2\theta_1'}{A_7} - \frac{12RdT_w\theta_0^2\theta_1'\,\theta_0'}{A_7}$$

Present address:
K. Sakkaravarthi, Department of Mathematics, St. Peter's Engineering College, Medchal, Dhulapally Hyderabad - 500100, Telangana, India.

$$+\frac{6RdT_w^{\,2}\theta_0\theta_1^{'}\theta_0^{'2}}{A_7}-\frac{12RdT_w\theta_0\theta_1\theta_0^{'2}}{A_7}+\frac{Rd\,\theta_1^{''}}{A_7}-3\theta_1^{''}+\frac{\theta_1^{'}}{\eta+K}+\frac{3RdT_w\theta_1\theta_0^{''}}{A_7}+\frac{6Rd\theta_1\theta_0^{''}}{A_7}$$
$$-\frac{3Rd\theta_0^{\,2}\theta_1\theta_0^{''}}{A_7}+\frac{3RdT_w\theta_0\theta_1^{''}}{A_7}+\frac{3RdT_w^{\,2}\theta_0^{\,2}\theta_1^{''}}{A_7}-\frac{6RdT_w\theta_0^{\,2}\theta_1^{''}}{A_7}-\frac{3RdT_w^{\,2}\theta_0^{\,3}\theta_1^{''}}{A_7}+\frac{3RdT_w\theta_0^{\,3}\theta_1^{''}}{A_7}$$
$$+\frac{3Rd\theta_0^{\,2}\theta_1^{''}}{A_7(\eta+K)}-\frac{3Rd\theta_0\theta_1^{'}}{A_7(\eta+K)}-\frac{Rd\theta_0\theta_1^{'}}{A_7(\eta+K)}+\frac{2Brf_0^{''}f_1^{'}}{A_7A_1}+\frac{6Rd\theta_0^{\,2}\theta_1^{'}}{A_7}-\frac{12Rd\theta_0^{'}\theta_1^{'}}{A_7}+\frac{6RdT_w\theta_1\theta_0^{'}}{A_7}$$
$$+\frac{6RdT_w\theta_1\theta_0^{'2}}{A_7}+\frac{6RdT_w^{\,3}\theta_1^{''}\theta_0^{\,3}}{A_7}-\frac{\gamma\,\mathrm{Pr}\,K^2f_0f_1\theta_0^{''}}{A_7(\eta+K)^2}-\frac{\gamma\,\mathrm{Pr}\,K^2f_0f^{'}{}_1\theta_1^{'}}{A_7(\eta+K)^2}--\frac{\gamma\,\mathrm{Pr}\,K^2f_0f^{'}{}_1\theta_0^{'}}{A_7(\eta+K)^2}=0 \quad (37)$$

Boundary conditions are

$$f_2(0)=S,\quad f_2{}'(0)=1+L_s\left(f_2{}''(0)-\frac{f_2{}'(0)}{K}\right),\quad f_2{}''(1)=0,\quad f_2{}'(1)=0.$$
$$\theta_2(0)=-Bi(1-\theta_2(0)),\quad \theta_2(1)=0 \quad (38)$$

HPM solutions take $f(\eta)$ and $\theta(\eta)$ into account predetermined dimensionless parameter values in $\phi_1=0.02$, $\phi_2=0.02$, Rd = 0.1, Ls = 0.5, $\gamma=0.02$, M = 1.0, $\lambda=0.1$, Bi = 0.3, Pr = 21, K = 0.5, $\lambda_1=0.1$, S_k = 0.2, $\chi_1=0.2$, $\chi_1=0.2$, $\alpha_1=0.1$, S = 0.5, $\theta_w=1.5$. The following outcomes are achieved by determining a succession of functions.

$$f(\eta)=\frac{1}{2\eta+1}(3.858024691\times10^{-17}(1.6661379670\times10^{12}\eta^7+1.181815725\times10^{14}\eta^6+2.094189598\times10^{16}\eta^4$$
$$-4.347271693\times10^{15}\times\ln(2\eta+1)\times\eta^4-1.063806241\times10^{15}\eta^5+1.915137715\times10^{16}\eta^3-2.085340034$$
$$\times10^{16}\ln(2\eta+1)\eta^3+6.200718999\times10^{16}\eta^2-3.880199531\times10^{16}\times\ln(2\eta+1)\times\eta^2+8.088966250\times10^{16}$$
$$-2.533558089\times10^{16}\ln(2\eta+1)\eta-5.302262184\times10^{16}\ln(2\eta+1)\eta-5.302262184\times10^{15}\ln(2\eta+1)$$
$$+2.59200000\times10^{16})) \quad (39)$$

$$\theta(\eta)=-0.9075255449\eta+0.3772321588+0.09968590234\eta^2+0.276492273643\ln(2\eta+1)\eta+0.1511897789\ln(2\eta+1)$$
$$-0.0000001715329004\eta^7+8.7134714334\times10^{-7}\eta^6+0.00041194224407\eta^5+0.0004505548475\eta^4$$
$$-0.01330311444\eta^3+0.005145987013e^{-\eta}\eta+1.0720806288\times0^{-7}\eta^8 \quad (40)$$

5.3. *Numerical Procedure*

Numerical methods are used to solve non-dimensional ODE equations as flows:

Present address:
K. Sakkaravarthi, Department of Mathematics, St. Peter's Engineering College, Medchal, Dhulapally Hyderabad - 500100, Telangana, India.

$$(1+\chi_1)\left(f^{iv}+2\frac{f'''}{\eta+K}-\frac{f''}{(\eta+K)^2}+\frac{f'}{(\eta+K)^3}\right)+A_2\left(\begin{array}{l}\frac{K}{\eta+K}\left(f'''f-f''f'\right)+\left(\frac{K}{(\eta+K)^2}\right)\left(f''f-f'^2\right)\\-\frac{K}{(\eta+K)^3}f'f\end{array}\right)$$

$$+3A_2\chi_1\chi_2\left(\frac{2f'f''f^{iv}}{K+\eta}-\frac{f''^2f^{iv}}{(K+\eta)^2}-f''^2f^{iv}\right)+\frac{A_2\chi_1\chi_2}{(K+\eta)}\left(6f'''f''^2+6f'''^2f'\right)-\frac{A_2\chi_1\chi_2}{(K+\eta)^2}\left(12f''f'f'''+3f'''^3\right)$$

$$-\frac{9A_2\chi_1\chi_2}{(K+\eta)^4}f''^2+\frac{3A_2\chi_1\chi_2}{(K+\eta)^5}f'^3+\frac{9A_2\chi_1\chi_2}{(K+\eta)^3}\left(6f'''f''^2+9f'f''^2\right)-6A_2\chi_1\chi_2f'''^2f''-A_1A_4M\left(\frac{f'}{(\eta+K)}+f''\right)$$

$$-S_k\left(\frac{f'}{(\eta+K)}+f''\right)+A_1A_5\lambda\left(\theta'+\frac{1}{(\eta+K)}\theta\right)=0$$

(41)

$$\left(\theta''+\frac{\theta'}{\eta+K}\right)\left(1+\frac{Rd}{A_7}\left(1+\left(\theta_w-1\right)\theta\right)^3\right)+\frac{3Rd}{A_7}\left[\left(1+\left(\theta_w-1\right)\theta\right)^2\right]\theta'^2+\frac{A_6}{A_7}Pr\left(\frac{K}{\eta+K}\right)f\theta'$$

$$+\frac{Br}{A_1A_7}\left(f''+\frac{f'}{\eta+K}\right)^2-\frac{\Pr}{A_7}\gamma\left(\frac{K^2}{\left(\eta+K\right)^2}\left(f^2\theta''+ff'\theta'\right)-K^2f^2\theta'\right)+\frac{A_4}{A_7}BrM\left(f'\right)^2+\frac{Pr}{A_7}\lambda_1\exp(-\eta)\theta=0$$

(42)

boundary conditions are

$$\left.\begin{array}{l}f(0)=S,\ -\theta'(0)=Bi(1-\theta(0)),\quad f'(0)=1+L_s\left(f''(0)-\frac{f'(0)}{K}\right)\\f''(\infty)=0,\quad f'(\infty)=0,\quad \theta(\infty)=0.\end{array}\right\}$$

(43)

In these above Eq. (41) - (42) uses the MAPLE software and R-K^{4th} order with the shooting method. As a result, the leading equations are solved in equations Eq. (43), along with their boundary conditions. Limiting asymptotic conditions in Eq. (43) $\eta\to\infty$ was revived by an imperfect set of efforts $\eta\eta$, say η a state in which there is no discernible variation in temperature, velocity, Bejan number, entropy production, or any other characteristic. In boundary layer studies, this is standard. Completed the problem-solving procedure, step scope with $\Delta\eta=0.01$ It's better to be realistic about the inward converging condition 10^{-6} under all circumstances.

6. Result and Discussion

Present address:
K. Sakkaravarthi, Department of Mathematics, St. Peter's Engineering College, Medchal, Dhulapally Hyderabad - 500100, Telangana, India.

This section is to study how different parameters affect velocity, temperature, entropy generation, and Bejan number profiles for the blood as the base fluid mixture with silver (*Ag)* and Ferrosoferric Oxide (Fe_3O_4) as the nanoparticles over a curved stretching sheet. It looks at how different parameters affect the velocity profile through a curved stretched sheet. The Temperature, Entropy generation and Bejan number of a hybrid nanofluid over a curved stretched sheet have been studied by comparing shapes (spheres, platelets, and blades). Additionally, investigated and shown in graphs are the skin friction and heat transfer coefficients. To compare results, we use the HPM. The Homotopy perturbation technique yields more accurate and consistent results than the numerical method. The results are most likely influenced by many parameters such as the curvature parameter (*K*), magnetic field parameter (*M*), porosity parameter (S_k), mixed convection parameter (λ), thermal radiation parameter (*Rd*), Brinkman number (*Br*), Thermal relaxation parameter(γ), Eyring-Powell parameters χ_1, χ_2, heat generation parameter (λ_1), dimensionless Biot number(*Bi*), silver (*Ag*) nanoparticle are volume fraction (ϕ_1), Ferrosoferric Oxide (Fe_3O_4) nanoparticles are volume fraction (ϕ_2), dimensionless slip parameter (*Ls*), the temperature ratio parameter (α_1), velocity profile $f'(\eta)$, temperature profile $\theta(\eta)$, entropy generation (S_G) and Bejan number (*Be*) is the shown in Figures 2-20. The HPM and NM are compared for temperature and velocity in Figures 2–3. The conclusions are based on previous results to validate the results obtained. The values of many dimensionless parameters are fixed in $\phi_1 = 0.02$, $\phi_2 = 0.02$, $Rd = 0.1$, $Ls = 0.5$, $\beta = 2.5$, $\gamma = 0.02$, $M = 1.0$, $\lambda = 0.1$, $Bi = 0.3$, $Pr = 21$, $K = 0.5$, $\lambda_1 = 0.1$, $S_k = 0.2$, $\alpha_1 = 0.1$, $\chi_1 = 0.2$, $\chi_1 = 0.2$, $S = 0.5$ and $\theta_w = 1.5$ are considered . The effects of the shape factors discussed for shapes like spheres, platelets, and blades are further represented by m = 3.0, 5.7, and 8.6, and hybrid nanoparticles are shown in Table 1.

6.1 Dimensionless velocity profiles

The influences of the M, χ_2 and S_k on the velocity profile are exposed in Figures 4-6. Figure 4 demonstrates that the velocity profile $f'(\eta)$ is a reducing function of the magnetic field (*M*) increases over a curved stretching sheet. Physically, when the magnetic field effect is improved, the Lorentz force increases, acting in the backward direction of the liquid flow and slowing the arrangement. So, when a curved sheet is stretched, increasing the magnetic

Present address:
K. Sakkaravarthi, Department of Mathematics, St. Peter's Engineering College, Medchal, Dhulapally Hyderabad - 500100, Telangana, India.

parameter slows down the $f'(\eta)$. Figure 5 demonstrates that the velocity profile $f'(\eta)$ is a reducing function of the Eyring-Powell fluid (χ_2). The velocity profile is decaying gradually for higher values χ_2. Figure 6 shows the impact of the porosity (S_k) curved stretching sheet on the hybrid nanofluid velocity profile has decreased. As the porosity variable (S_k) rises, so does the friction force between nanoparticles. Physically, increasing porosity causes the medium's pore size to decrease.

6.2. *Dimensionless temperature profiles*

The influences of the thermal radiation (*Rd*), thermal relaxation (γ), heat generation (λ_1), Brinkman number (*Br*), and Biot number (*Bi*) on the comparing shapes (spheres, platelets, and blades) over a curved stretched sheet at the temperature profile $\theta(\eta)$ are shown in Figures 7–9. The highlights of thermal radiation (*Rd*) on hybrid nanofluid temperature profiles are conveyed in Figure 7. As the thermal radiation increases, the temperature profile increases for comparison shapes (spheres, platelets, and blades). When the mean absorption coefficient is reduced due to an increase in the thermal radiation parameter *Rd*, more heat is transmitted in the fluid direction as the fluid temperature rises. Figure 8 depicts the thermal relaxation parameter (γ) for comparison shapes by increasing the values as the temperature profile $\theta(\eta)$ decreases. Physically, inclined (γ) material particles need more time to transfer heat to their contiguous particles. Also, inclination in (γ) the material has a non-conducting effect that leads to the loss of a thermal relaxation parameter. The highlights of the heat generation parameter (λ_1) on hybrid nanofluid flow temperature profiles $\theta(\eta)$ on the shapes (spheres, platelets, and blades) are conveyed in Figure 9. Physically, the fluid will get more heat from the surface. As a result, raising the heat generation value causes the temperature profile $\theta(\eta)$ to rise.

6.3. *Entropy generation*

In Figures 10–13, the comparison of shapes (spheres, platelets, and blades) over a curved stretched sheet at the entropy generation S_G is shown for several influence parameters such as *Rd*, *Bi*, and *Br*. Figure 10 illustrates the impact of *Rd* on the entropy generation S_G of hybrid nanofluid for the curved stretching sheet. When the thermal radiation grows, the three shapes increase in entropy generation. physically, Growing the thermal radiation emission

Present address:
K. Sakkaravarthi, Department of Mathematics, St. Peter's Engineering College, Medchal, Dhulapally Hyderabad - 500100, Telangana, India.

increases the disorder in the closed system, causing the radiative constant to rise. As a result, the system's entropy rate increases. The effect of the *Br* on the S_G profile is seen in Figure 11. Entropy generation rises in three different shapes, As *Br* rises. A higher Brinkman number increases the viscous force, resulting in increased collisions between fluid particles. As a result, the entropy rate has increased. Figure 12 shows the effect of the Biot number *(Bi)* on the entropy generation for the curved stretching sheet. The S_G grows in three shapes as the Biot number increases.

6.4. ***Bejan number***

Figures 13 - 15 compare the shapes like spheres, platelets, and blades over a curved stretched sheet at the *Be* for different parameters such as *M* and *Rd*. Figure 13 shows the influence of the magnetic field parameter on the Bejan number. The Bejan number decreases in three shapes as the magnetic field increases. This is because stronger magnetic fields tend to have more Lorentz force acting on fluid motion. Bejan number (*Be*) is reduced versus larger values of magnetic field (*M*). Figure 14 demonstrates the effect of the thermal Radiation (*Rd)* parameter on the Bejan number. As the thermal radiation rises, the Bejan number increases in three shapes. Growing the thermal radiation emission increases the disorderedness in the closed system, causing the radiative constant to rise. As a result, the Bejan number of the system rises.

Figure 15 depicts the impact of the Biot number on the Bejan number, the *Be* increases in three shapes as the Biot number *(Bi)* increases. It has been shown that the viscous consequence has a greater impact on physical strength than thermal irreversibility.

6.5. ***Physical quantities***

In Figures 16 and 17 the effect of ϕ_1, ϕ_2 and *M* on $C_{fs}\,\mathrm{Re}_s^{1/2}$ Eyring-Powell hybrid nanofluid is used to investigate the impact of the $C_{fs}\,\mathrm{Re}_s^{1/2}$ different hybrid nanoparticle volume fraction values ϕ_1, ϕ_2 and *M*, respectively. It's been seen that the $C_{fs}\,\mathrm{Re}_s^{1/2}$ is a growing function of ϕ_1, ϕ_2 and *M*. The increase in skin friction is due to the thermal conductivity of nanoparticles, which is improved by growth estimates of the nanoparticle volume fraction. Figure 18 shows that the effect of ϕ_1 and thermal radiation parameter (*Rd*) on $C_{fs}\,\mathrm{Re}_s^{1/2}$ Eyring-Powell hybrid nanofluid is used to investigate the impact of the $C_{fs}\,\mathrm{Re}_s^{1/2}$ different hybrid nanoparticle volume fraction values ϕ_1 and thermal radiation parameter (*Rd*)

Present address:
K. Sakkaravarthi, Department of Mathematics, St. Peter's Engineering College, Medchal, Dhulapally Hyderabad - 500100, Telangana, India.

respectively. It is seen that the $C_{fs}\,\mathrm{Re}_s^{1/2}$ is enhancing the performance of ϕ_1 and *Rd*. In Figures 19 and 20 the effect of ϕ_1, ϕ_2 and thermal radiation parameter (*Rd*) on $Nu_s\,\mathrm{Re}_s^{-1/2}$ Eyring-Powell hybrid nanofluid is used to investigate the impact of the $Nu_s\,\mathrm{Re}_s^{-1/2}$ different hybrid nanoparticle volume fraction values ϕ_1, ϕ_2 and thermal radiation parameter (*Rd*), correspondingly. It is shown that the $Nu_s\,\mathrm{Re}_s^{-1/2}$ is an increasing productivity function of ϕ_1, ϕ_2 and *Rd*. Table 2 demonstrates that the present approach corresponds more closely with Okechi et al.[28] and Ahmed et al.[29] solutions based on prior work. Which received a good agreement. This suggests that the HPM simulation used produces reliable findings.

7. Conclusion

This article investigates the entropy generation in an MHD Eyring-Powell hybrid nanofluid (*Ag- Fe_3O_4*/ Blood) over a curved stretched sheet, as well as the effect of shape factors (spheres, platelets, and blades). Investigated were the effects of the porous medium, heat generation, nonlinear thermal radiation, the Cattaneo-Christov heat flux model, mixed convection, and bioconvective boundary conditions. In comparison to the Numerical Method, the Homotopy Perturbation Method (HPM) generates more dependable and accurate results, which can be represented by graphs and tables. This model is related to radiation therapy and is one of the most effective methods for treating cancer or hyperthermia. This technology employs silver and a magnetic particle to treat cancer without harming other organs. It is reasonable and prudent to draw that conclusion.

- When a magnetic field influenced the hybrid nanofluid increase over a curved stretching sheet, the velocity profile was reduced. In reality, the Lorentz force increases as the magnetic field effect is amplified, acting against the flow of the liquid to slow the system down. In the presence of a curved stretching sheet, the velocity profile also decreases as a result of increased magnetic parameters.
- As Eyring-Powell and porosity are enhanced, the profile of velocity decreases.
- As thermal relaxation increases, the shape of the temperature profile diminishes (spheres, platelets, and blades). The hybrid nanofluid particles that

Present address:
K. Sakkaravarthi, Department of Mathematics, St. Peter's Engineering College, Medchal, Dhulapally Hyderabad - 500100, Telangana, India.

are physically inclined require more time to transfer heat to their contiguous particles. In addition, the inclination of the material in (γ) results in the loss of a thermal relaxation parameter due to a non-conducting effect.

- As thermal radiation increases, the temperature profile for comparing shapes (spheres, platelets, and blades) rises. An increase in the thermal radiation parameter *Rd* reduces the average absorption coefficient. As fluid temperature rises, more heat is transferred in the fluid's direction.
- As the magnetic field parameter increases, three distinct forms of entropy are produced. Physically, increasing the magnetic parameter and Lorentz force at the same time increases abrasion, thereby increasing entropy production.
- As the influence of the thermal radiation parameters and *Bi* increases, the Bejan number contour rises.
- In conclusion, I offer the following suggestions for the future: Various non-Newtonian fluids can be considered with a variety of boundary conditions. I attempt to solve base fluid and nanofluid ternary-hybrid.

References

1. Choi, S. U. S., "Enhancing thermal conductivity of fluids with nanoparticles", *Am. Soc. Mech. Eng. Fluids Eng. Div. FED*, **231**(March), pp. 99–105 (1995).

2. Saba, F., Ahmed, N., Khan, U., et al., "International Journal of Heat and Mass Transfer A novel coupling of ð CNT À Fe 3 O 4 = H 2 O Þ hybrid nanofluid for improvements in heat transfer for flow in an asymmetric channel with dilating / squeezing walls", *Int. J. Heat Mass Transf.*, **136**, pp. 186–195 (2019).

3. Madhukesh, J. K., Naveen Kumar, R., Punith Gowda, R. J., et al., "Numerical simulation of AA7072-AA7075/water-based hybrid nanofluid flow over a curved stretching sheet with Newtonian heating: A non-Fourier heat flux model approach", *J. Mol. Liq.*, **335**, p. 116103 (2021).

4. Shah, M., Badwaik, V. D., and Dakshinamurthy, R., "Biological applications of gold nanoparticles", *J. Nanosci. Nanotechnol.*, **14**(1), pp. 344–362 (2014).

Present address:
K. Sakkaravarthi, Department of Mathematics, St. Peter's Engineering College, Medchal, Dhulapally Hyderabad - 500100, Telangana, India.

5. Lacerda, S. H. D. P., Park, J. J., Meuse, C., Pristinski, D., et al., "Interaction of Gold Nanoparticles with Common Human Blood Proteins", **4**(1), pp. 365–379 (2010).

6. Kumar, K. G., Reddy, M. G., Vijaya kumari, P., et al., "Application of different hybrid nanofluids in convective heat transport of Carreau fluid", *Chaos, Solitons and Fractals*, **141** (2020).

7. Abbas, N., Ur, K., Shatanawi, W., and Malik, M. Y., "Numerical study of heat transfer in hybrid nanofluid flow over permeable nonlinear stretching curved surface with thermal slip", *Int. Commun. Heat Mass Transf.*, **135**(May), p. 106107 (2022).

8. Babu, M. J., Rao, Y. S., Kumar, A. S., et al., "Squeezed flow of polyethylene glycol and water based hybrid nanofluid over a magnetized sensor surface: A statistical approach", *Int. Commun. Heat Mass Transf.*, **135**, p. 106136 (2022).

9. Asogwa, K. K. and Shankar Goud, B., "Impact of velocity slip and heat source on tangent hyperbolic nanofluid flow over an electromagnetic surface with Soret effect and variable suction/injection", *Proc. Inst. Mech. Eng. Part E J. Process Mech. Eng.* (2022).

10. Sajjan, K., Shah, N. A., Ameer Ahammad, N., et al., "Nonlinear Boussinesq and Rosseland approximations on 3D flow in an interruption of Ternary nanoparticles with various shapes of densities and conductivity properties", *AIMS Math.*, **7**(10), pp. 18416–18449 (2022).

11. Mahabaleshwar, U. S., Sneha, K. N., and Huang, H. N., "An effect of MHD and radiation on CNTS-Water based nanofluids due to a stretching sheet in a Newtonian fluid", *Case Stud. Therm. Eng.*, **28**(September), p. 101462 (2021).

12. Islam, S., Jawad, M., Gokul, K. C., et al., "Entropy optimization in mhd nanofluid flow over a curved exponentially stretching surface with binary chemical reaction and arrhenius activation energy", *J. Phys. Commun.*, **4**(7), pp. 1–25 (2020).

13. Sakkaravarthi, K. and Reddy, P. B. A., "Entropy optimization of MHD hybrid nanofluid flow through a curved stretching sheet with thermal radiation and heat generation: Semi-analytical and numerical simulations", *Proc. Inst. Mech. Eng. Part E*

Present address:
K. Sakkaravarthi, Department of Mathematics, St. Peter's Engineering College, Medchal, Dhulapally Hyderabad - 500100, Telangana, India.

J. Process Mech. Eng., pp. 1–11 (2022).

14. Jalili, B., Jalili, P., Sadighi, S., et al., "Effect of magnetic and boundary parameters on flow characteristics analysis of micropolar ferrofluid through the shrinking sheet with effective thermal conductivity", *Chinese J. Phys.*, **71**(September 2019), pp. 136–150 (2021).

15. Reddy, S. C., Asogwa, K. K., Yassen, M. F., et al., "Dynamics of MHD second-grade nanofluid flow with activation energy across a curved stretching surface", *Front. Energy Res.*, **10**(October), pp. 1–12 (2022).

16. Rauf, A., Ali Shah, N., Mushtaq, A., et al., "Heat transport and magnetohydrodynamic hybrid micropolar ferrofluid flow over a non-linearly stretching sheet", *AIMS Math.*, **8**(1), pp. 164–193 (2023).

17. Ashraf, M. Z., Rehman, S. U., Farid, S., et al., "Insight into Significance of Bioconvection on MHD Tangent Hyperbolic Nanofluid Flow of Irregular Thickness across a Slender Elastic Surface", *Mathematics*, **10**(15), pp. 1–17 (2022).

18. Jakeer, S. and Anki Reddy, B., "Competence of magnetic dipole and radiation on permeable surface using prescribed heat flux / prescribed surface temperature and homogeneousheterogeneous reactions", *Spec. Top. Rev. Porous Media An Int. J.*, **12**(6), pp. 91–107 (2021).

19. Ahmed, N., Saba, F., Khan, U., et al., "Nonlinear thermal radiation and chemical reaction effects on a (Cu-Cuo)/NaAlg hybrid nanofluid flow past a stretching curved surface", *Processes*, **7**(12) (2019).

20. Sakkaravarthi, K. and Reddy, P. B. A., "Entropy generation on Casson hybrid nanofluid over a curved stretching sheet with convective boundary condition: Semi-analytical and numerical simulations", *Proc. Inst. Mech. Eng. Part C J. Mech. Eng. Sci.* (2022).

21. Jalili, P., Kazerani, K., Jalili, B., et al., "Investigation of thermal analysis and pressure drop in non-continuous helical baffle with different helix angles and hybrid nano-particles", *Case Stud. Therm. Eng.*, **36**(June), p. 102209 (2022).

Present address:
K. Sakkaravarthi, Department of Mathematics, St. Peter's Engineering College, Medchal, Dhulapally Hyderabad - 500100, Telangana, India.

22. Bejan, A., “A study of entropy generation in fundamental convective heat transfer”, *J. Heat Transfer*, **101**(4), pp. 718–725 (1979).

23. Hayat, T., Khan, S. A., Alsaedi, A., et al., “Irreversibility analysis in Darcy-Forchheimer flow of CNTs with dissipation and Joule heating effects by a curved stretching sheet”, *Appl. Nanosci.*, **11**(1), pp. 187–198 (2021).

24. Hayat, T., Khan, S. A., Alsaedi, A., et al., “Computational analysis of heat transfer in mixed convective flow of CNTs with entropy optimization by a curved stretching sheet”, *Int. Commun. Heat Mass Transf.*, **118**(September), p. 104881 (2020).

25. Jakeer, S. and Bala Anki Reddy, P., “Entropy generation on EMHD stagnation point flow of hybrid nanofluid over a stretching sheet: Homotopy perturbation solution”, *Phys. Scr.*, **95**(12), p. 125203 (2020).

26. He, J. H., “Comparison of homotopy perturbation method and homotopy analysis method”, *Appl. Math. Comput.*, **156**(2), pp. 527–539 (2004).

27. Shqair, M., “Solution of different geometries reflected reactors neutron diffusion equation using the homotopy perturbation method”, *Results Phys.*, **12**(September 2018), pp. 61–66 (2019).

28. Okechi, N. F., Jalil, M., and Asghar, S., “Flow of viscous fluid along an exponentially stretching curved surface”, *Results Phys.*, **7**, pp. 2851–2854 (2017).

29. Ahmed, K., Khan, W. A., Akbar, T., et al., “Numerical investigation of mixed convective williamson fluid flow over an exponentially stretching permeable curved surface”, *Fluids*, **6**(7) (2021).

30. Divya, A. and Reddy, P. B. A., “Electromagnetohydrodynamic unsteady flow with entropy generation and hall current of hybrid nanofluid over a rotating disk: An application in hyperthermia therapeutic aspects”, *Proc. Inst. Mech. Eng. Part C J. Mech. Eng. Sci.* (2022).

Biographies

Present address:
K. Sakkaravarthi, Department of Mathematics, St. Peter's Engineering College, Medchal, Dhulapally Hyderabad - 500100, Telangana, India.

Dr. K. Sakkaravarthi was born and brought up in Tamil Nadu, India. He obtained his M.Sc. from Kongunadu Arts &Science College, Coimbatore, Tamil Nadu, India. He obtained his M.Phil. degree at Govt Arts College Tiruvannamalai. He obtained his B.Ed. degree at Arunachala College of Education, Tiruvannamalai, Tamil Nadu, India. Presently, he is working as an assistant professor at St. Peter's Engineering College, Hyderabad. He has more than 10 years of teaching and research experience. His research interests cover areas of the application of flow separation, particularly bio-fluid dynamics and the analysis of boundary layer flows in Newtonian and non-Newtonian fluids, including heat and mass transfer in porous and non-porous media. His research interests also cover nanofluid, hybrid, and ternary hybrid flow problems with entropy generations. He published four papers in national and international journals.

Dr. P. Bala Anki Reddy was born and brought up in Andhra Pradesh, India. He obtained his M.Sc. and Ph.D. degrees in Mathematics from Sri Venkateshwara University, Tirupati, Andhra Pradesh. Presently, he is working as an Associate Professor in the Department of Mathematics at VIT University, Vellore, Tamil Nadu. His research interests cover areas of the application of flow separation, particularly bio-fluid dynamics and the analysis of boundary layer flows in Newtonian and non-Newtonian fluids, including heat and mass transfer in porous and non-porous media. His research interests also cover nanofluid flow problems with entropy generations. He published several papers in national and international journals. He attended several workshops, seminars, and faculty development programs. Also, Reddy was recognised as a Top 2% Scientist in the World by Stanford University, USA, and Elsevier BV for the years 2022 and 2023 (single year). Moreover, Reddy received the Top1% citation award from IOP publications for the year 2023.

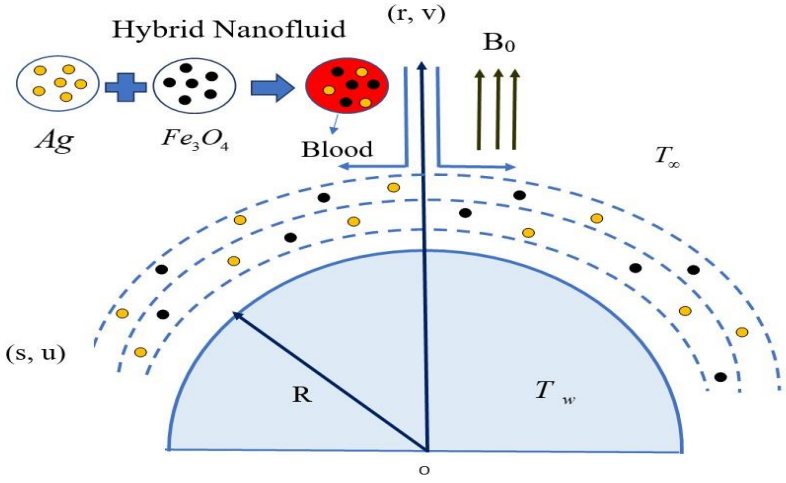

Pres
K. S
Dhu

Figure 1. Hybrid nanofluid flow is shown on a curved stretching sheet.

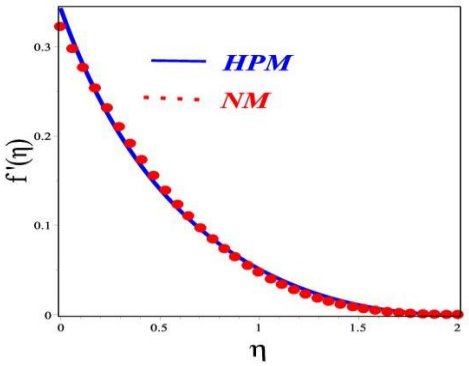

Figure 2. Comparisons of the R-K method with the HPM for velocity profile.

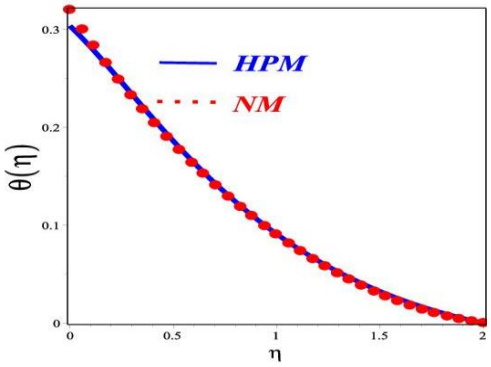

Figure 3. Comparisons of the R-K method with the HPM for Temperature profile.

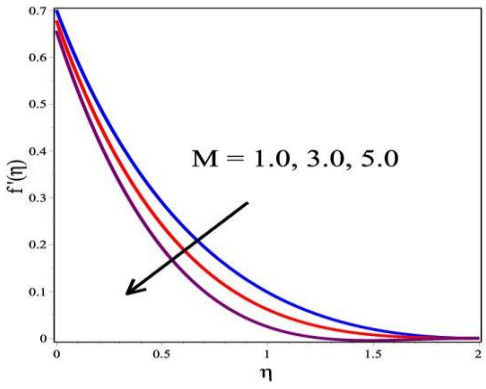

Figure 4. The behaviour of $f'(\eta)$ with different values of *M*.

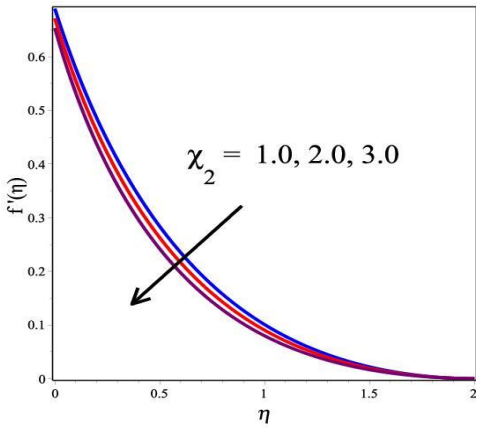

Figure 5. The behaviour of $f'(\eta)$ with specific values of χ_2 .

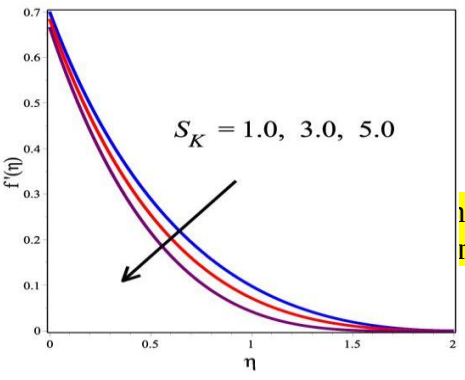

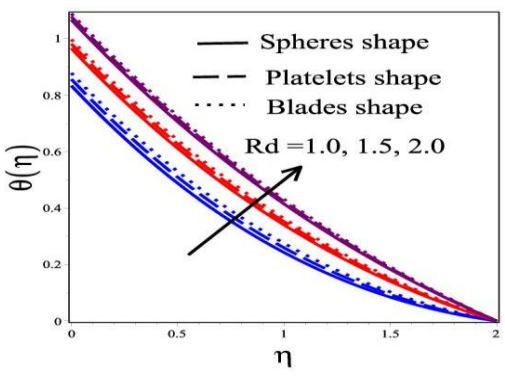

Figure 6. The behaviour of $f'(\eta)$ with specific values of S_K.

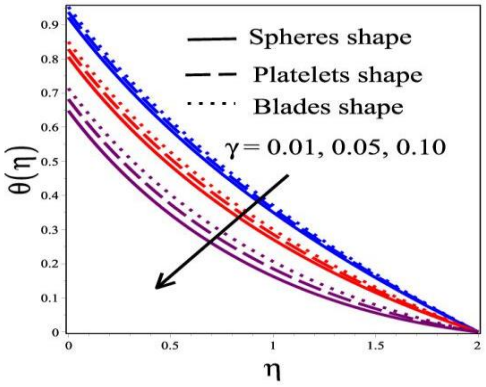

Figure 8. The behaviour of $\theta(\eta)$ with specific values of γ .

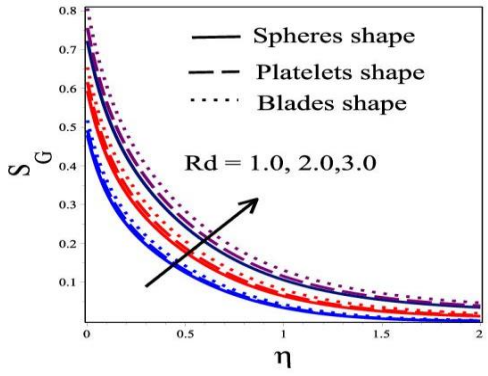

Figure 10. The behaviour of S_G with specific values of Rd.

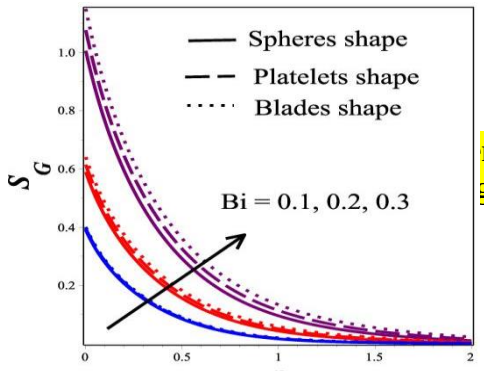

Figure 7. The behaviour of $\theta(\eta)$ with specific values of *Rd.*

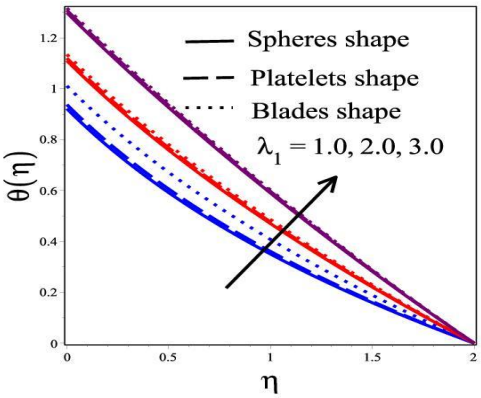

Figure 9. The behaviour of $\theta(\eta)$ with specific values of λ .

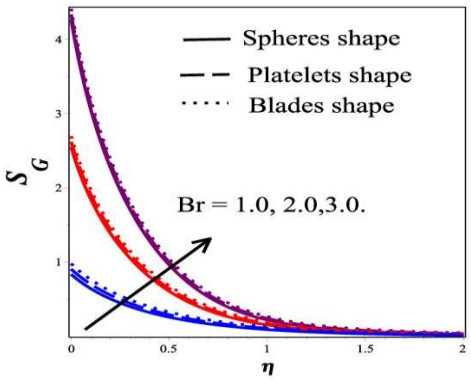

Figure 11. The behaviour of S_G with specific values of Br.

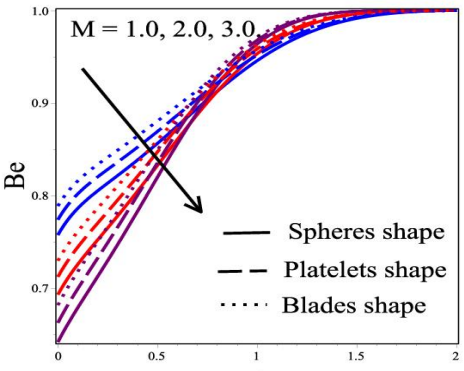

P
K
D
matics, St. Peter
gana, India.

Figure 12. The behaviour of S_G with specific values of *Bi*.

Figure 13. The behaviour of *Be* with specific values of *M*.

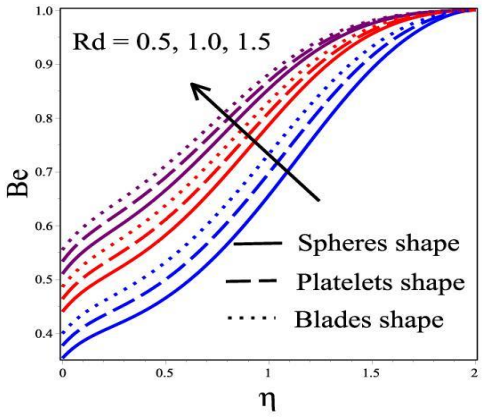

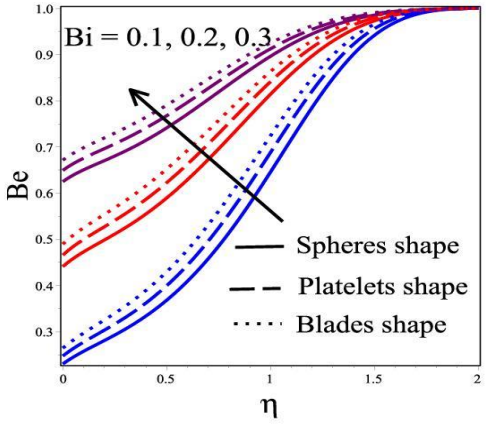

Figure 14. The behaviour of *Be* with specific values of *Rd*.

Figure 15. The behaviour of *Be* with specific values of *Bi*.

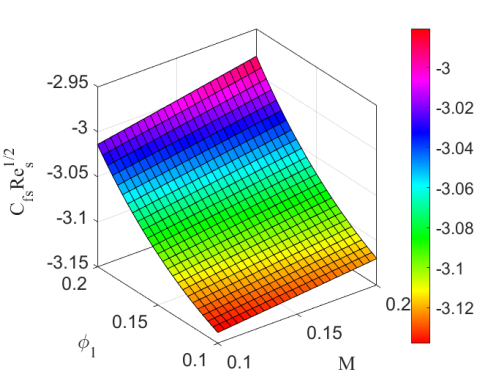

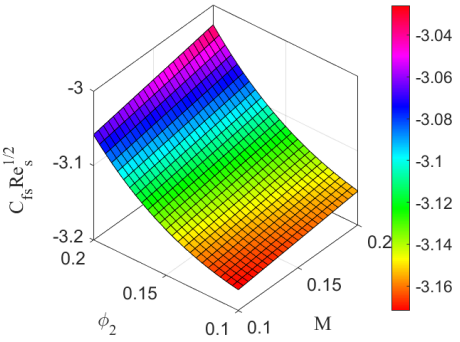

Figure 16. The Variant of ϕ_1 and M on $C_{fs}\,\mathrm{Re}_s^{1/2}$

Figure 17. The Variant of ϕ_2 and M on $C_{fs}\,\mathrm{Re}_s^{1/2}$

Present address:
K. Sakkaravarthi, Department of Mathematics, St. Peter's Engineering College, Medchal, Dhulapally Hyderabad - 500100, Telangana, India.

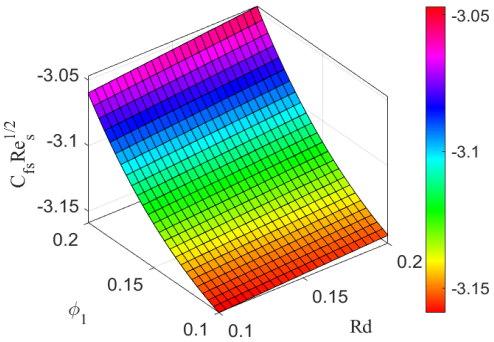

Figure 18. The variant of ϕ_1 and Rd on $C_{fs}\,\mathrm{Re}_s^{1/2}$

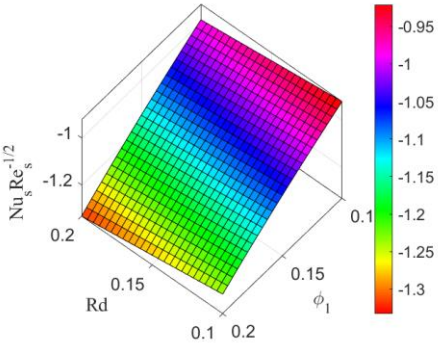

Figure 19. The Variant of ϕ_1 and Rd on $Nu_s\,\mathrm{Re}_s^{-1/2}$

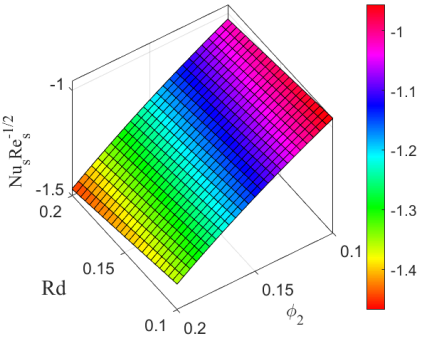

Figure 20. The Variant of ϕ_2 and Rd on $Nu_s\,\mathrm{Re}_s^{-1/2}$

Table 1. shows the thermo-physical properties of blood as a base fluid and nanoparticles are silver (*Ag*) and Ferrosoferric Oxide (Fe_3O_4): Divya and Reddy [30]

Property	Blood (b_f)	Silver *Ag* (1s)	Ferrosoferric Oxide Fe_3O_4 (2s)
$\rho\left(kg/m^3\right)$	1063	10500	5180
$c_p\left(J/kgK\right)$	3594	235	670
$k\left(W/mk\right)$	0.492	429	9.7
$\sigma\left(s/m\right)$	0.8	6.30×10^7	0.025×10^7
$\beta\times10^{-6}\left(K^{-1}\right)$	0.18	1.89	1.3
Pr		-	-

Present address:
K. Sakkaravarthi, Department of Mathematics, St. Peter's Engineering College, Medchal, Dhulapally Hyderabad - 500100, Telangana, India.

Table 2. Adjustments *K* to compare the Skin-friction coefficient.

The radius of curvature parameters	Okechi *et al*. [28]	Ahmed *et al*. [29]	Current result
5	1.41960	1.41970	1.41970
10	1.34670	1.34690	1.34680
20	1.31350	1.31360	1.31350
30	1.30280	1.30280	1.30280
40	1.29750	1.29750	1.29720
50	1.29440	1.29440	1.29460
100	1.28810	1.28810	1.28890

NOMENCLATURE			
A	Constant	T_W	Wall Temperature
B_0	Strengthening magnetic field	T_∞	Faraway
Be	Bejan number	u	Component of s-direction velocity
Br	Brinkman number	v	Component of r-direction velocity
$C_{fs}\,\mathrm{Re}_s^{1/2}$	Skin friction coefficient	Greek symbols	
c_p	Specific heat	ρ	Fluid density
Ec	Eckert number	μ	Dynamic viscosity
S_k	Porosity parameter	α_1	Temperature ratio parameter
k	Thermal conductivity	ν	Kinetic viscosity
g	Gravity	σ	Electrical conductivity
L	Slip length	θ	The dimensionless Temperature of a fluid
L_s	Dimensionless slip parameter	η	Similarity variable
M	Magnetic field parameter	σ^*	Stefan-Boltzmann constant
$\hat{p}$	Hybrid nanofluid Pressure	λ	Mixed Convection parameter
P	Hybrid nanofluid Dimensionless Pressure	λ_1	Heat generation parameter
Pr	Prandtl number	k^*	Mean absorption coefficient
Q	Heat source /sink	ϕ_1, ϕ_2	Hybrid nanoparticles

Present address:
K. Sakkaravarthi, Department of Mathematics, St. Peter's Engineering College, Medchal, Dhulapally Hyderabad - 500100, Telangana, India.

			volume fractions
q_r	Heat flux radiative	Subscripts	
R	Radius of curvature	b_f	Base fluid
Rd	Thermal radiation parameter	hnf	Hybrid nanofluid
S_G	Total entropy rate	$1s$	First particle
T	The temperature at the surface	$2s$	Second particle.

Present address:
K. Sakkaravarthi, Department of Mathematics, St. Peter's Engineering College, Medchal, Dhulapally Hyderabad - 500100, Telangana, India.